Porosity Formation by Biaxial Stretching in Polyolefin Films Filled with Calcium Carbonate Particles

A. Qaiss,[1,2] H. Saidi,[2,3,4] O. Fassi-Fehri,[4,5] M. Bousmina[1,4,5]

[1]*Canada Research Chair on Polymer Physics and Nanomaterials, Department of Chemical Engineering, Laval University, Ste-Foy, Québec, G1K 7P4, Canada*
[2]*INANOTECH (Institute of Nanomaterials and Nanotechnology), ENSET, Av. Des FARS, Madinat Al Irfane, 10100, Hay Riad, Rabat, Morocco*
[3]*LPHE-Modélisation et Simulation, Faculté des Sciences, Université MV-Agdal, Rabat, Morocco*
[4]*Hassan II Academy of Science and Technology, Rabat, Morocco*
[5]*Laboratoire de physique et mécanique des matériaux, Faculté des Sciences, Université MV-Agdal, Rabat, Morocco*

Received 29 June 2010; accepted 4 April 2011
DOI 10.1002/app.34612
Published online 15 September 2011 in Wiley Online Library (wileyonlinelibrary.com).

ABSTRACT: Porous polymer films were generated by biaxial stretching of polypropylene (PP) and high-density polyethylene (HDPE) filled with various amounts of calcium carbonate particles. The porosity of the films was measured by mercury porosimetry, and the obtained results were related to the processing conditions and to the morphology development during the biaxial stretching. The results showed that increasing the calcium carbonate ($CaCO_3$) concentration and the draw ratio resulted in porosity increase for PP-based composite films and in a decreased porosity in HDPE-based composite films. Such peculiar behavior was connected to interfacial specific interactions between the matrix and the dispersed particles as well as to the crystallinity of the films. © 2011 Wiley Periodicals, Inc. J Appl Polym Sci 123: 3425–3436, 2012

Key words: porosity; biaxial stretching; cystallinity

INTRODUCTION

Polymeric films with non-interconnected porous structure are generally obtained by several foaming techniques using various liquids, solids, and gas foaming agents.[1,2] Alternative routes include mechanical stretching with the presence of dispersed particles under various draw ratios.[3–6] Biaxial stretching of polymer films loaded with fine particles offers the possibility of generating various cell sizes and densities depending on the particle size that can range from few nanometers to some hundreds of microns, the processing conditions such as temperature, draw ratio, and rate of stretching as well as polymer characteristics (film thickness, crystallinity, and thermomechanical properties) and the polymer–particle interfacial properties.

Such thin polymeric films with closed pores have been recently used for high-tech applications such as piezoelectric films for the fabrication of sensors, actuators, and transducers. The piezoelectric behavior in such structured cellular thin films is generally obtained by filling the cells with an inert gas under pressure and then ionizing it under high-voltage electric field to generate a distribution of negative and positive charges at the inner surface of the cells. The electrically charged cells develop local electrical dipoles that generate an electrical signal (voltage or current) when the polymeric film is submitted to an external mechanical stimulus.[7–9]

Porosity formation during stretching is due to local stresses' concentration at the surface of the particles that produces decohesion at the matrix–particle interface. The presence of solid particles within the homogeneous polymeric matrix initiates and facilitates the formation of cracks due to stress concentration around the surface of the particles as sketched in Figure 1 for unixial stretching. Within the polymeric matrix, the stress lines are homogeneous, while in the close vicinity of particles, the lines are curved with a higher density, which represents the high level of stress concentration. The stress concentration may be quantitatively characterized by:

$$K_t = \frac{\sigma_{act}}{\sigma_{nom}}, \quad (1)$$

where σ_{real} is the actual stress, and σ_{nom} is the nominal stress shown in Figure 1. For a given type of leading, the theoretical coefficient K_t gives the ratio of the actual stress to the nominal stress at a given

Correspondence to: M. Bousmina (bousmina@gch.ulaval.ca).

Contract grant sponsors: NSERC (National Science and Engineering Research Council of Canada), Canada Research Chair on Polymer Physics and Nanomaterials, Hassan II Academy of Science and Technology, Morocco.

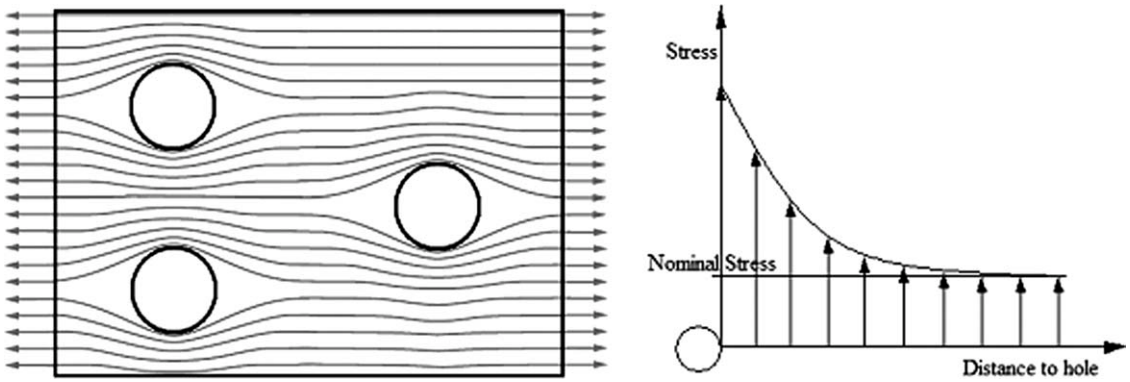

Figure 1 Qualitative diagrammatic illustration showing the origin of the stress concentration.

point and does not depend on the value of the applied load (nominal stress).

It is important to mention that the theoretical value of this coefficient is based on the assumptions of the elasticity theory, and it will be used here as an indicator allowing the explanation of the stress concentration phenomenon, albeit the plastic deformations that characterize the mechanical properties of the films studied in this work.

The expression of the stress concentration coefficient[10,11] for simple shapes subjected to a uniaxial stress (traction) is given by

$$K_t = 1 + 2\sqrt{\frac{a}{\rho}}, \tag{2}$$

where a the half length of the notch, and ρ the curvature radius of the notch. In the case of a hole, a is equal to ρ, which gives $K_t = 3$.

In this work, a direct use of stress concentration is presented with the objective of developing porous structures with non-interconnected pores, using various percentages of calcium carbonate particles, $CaCO_3$, dispersed within two polyolefin matrices (HDPE and PP). The porosity was generated by biaxial stretching using a home-developed device at various draw ratios, and the obtained porosity was evaluated by scanning electron microscopy and by mercury porosimetry. The overall results are discussed in terms of cell structure, initial free volume, cristallinity, and molecular rearrangements during stretching.

TABLE I
Characteristics of PP and HDPE

	Density ρ (g/cm^3)	Melting point (°C)	Thermal conductivity k (W/mK)	Specific heat capacity Cp (kJ/(kg K))
PP[12]	0.905	164	0.12	1.622
HDPE[13]	0.960	130	0.52	1.555

EXPERIMENTS

Materials

The experiments were carried out using a high-density polyethylene (HDPE) and a polypropylene (PP). The two polymers were selected due to their high-mechanical strength and the possibility to process them in the form of thin films. PP and HDPE were purchased from Basell Canada under the trade names of Pro-fax PDC 1274 and H6018, respectively. Some of their characteristics are reported in Table I.

The two polymers were filled with 5, 10, and 15 wt % of calcium carbonate, $CaCO_3$, particles of $\sim$ 10-μm granulometry, purchased from Sigma Aldrich. The choice of $CaCO_3$ was based on its wide availability, on its low price, and on the morphology of its particles having sharp edges that favor the concentration of stresses (Fig. 2), and thus, the propagation of microscopic cracks that finally lead to controlled pore sizes using the relationship (2). In this case, the $CaCO_3$ particles were assumed to have ellipsoidal shape (Fig. 2), with $a = 15$ μm and $\rho = 1.5$ μm. When the film is stressed in x direction, the initial stress

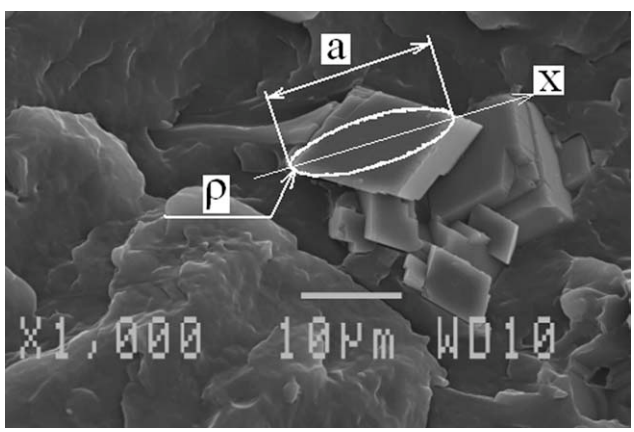

Figure 2 Scanning electron micrographs PP matrix charged by $CaCO_3$ particles.

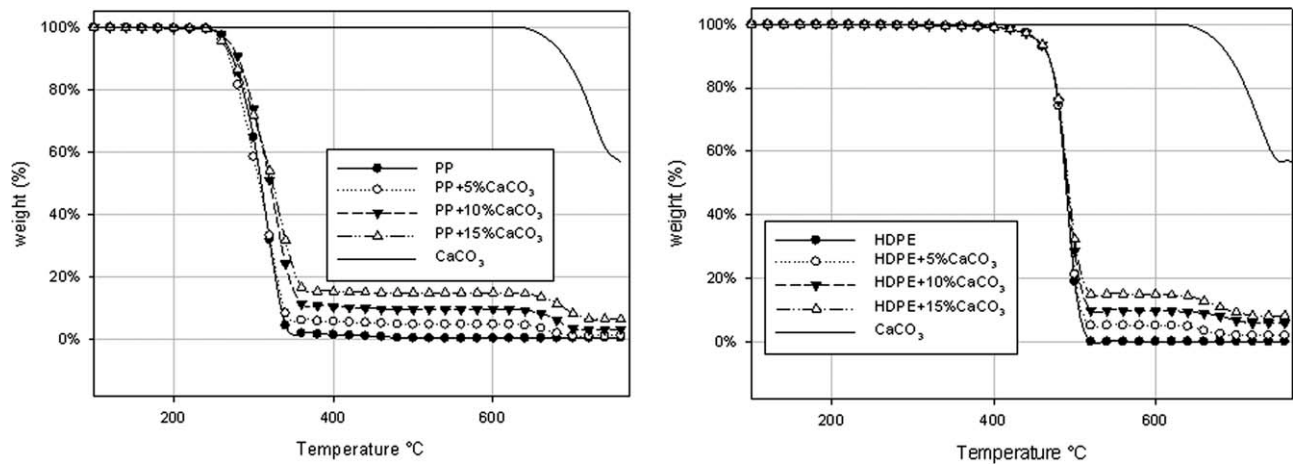

Figure 3 TGA analyses of films with 0, 5, 10, and 15% load in $CaCO_3$.

concentration coefficient is equal to 7.32 [using the relationship (2)].

Extrusion of filled-polymeric films

The polymers in form of granules and $CaCO_3$ in form of powder with various weight percents (5, 10, and 15 wt %) were extruded altogether using the corotating twin-screw extruder machine (model ZSE27) with modulated screw $d = 27$mm, having a length to diameter ratio of 40 and 9 heating zones. The extruder screws were configured to ensure a better distribution of $CaCO_3$ particles within the polymeric matrix. The granules were supplied in zone 0 using a mass control feeder, while addition of $CaCO_3$ was ensured by a suitable feeder for powders that feeds a side-stuffer located in the fourth zone. The feed rate for the two types of matrices (HDPE and PP) was of 2kg/h. For HDPE, the temperature profile in the various zones along the extruder was 165, 165–170, and 170°C at the die; whereas for PP, the profile was 180, 190–185, and 180°C in the die.

The outlet side of the extruder was equipped with a die punt to adjust its opening and, therefore, to control the extruded film thickness. The adjustment of the punt opening along with the use of a calendaring system with a heating temperature of 90°C for HDPE and 100°C for PP allowed obtaining films with 500 μm in thickness. The percentage of $CaCO_3$ in the polymeric composite films was checked by thermogravimetric analysis shown in Figure 3. In fact, the figure shows that after the polymer degradation, the percentage of the remaining solid coincides with the initial fixed percentage of $CaCO_3$.

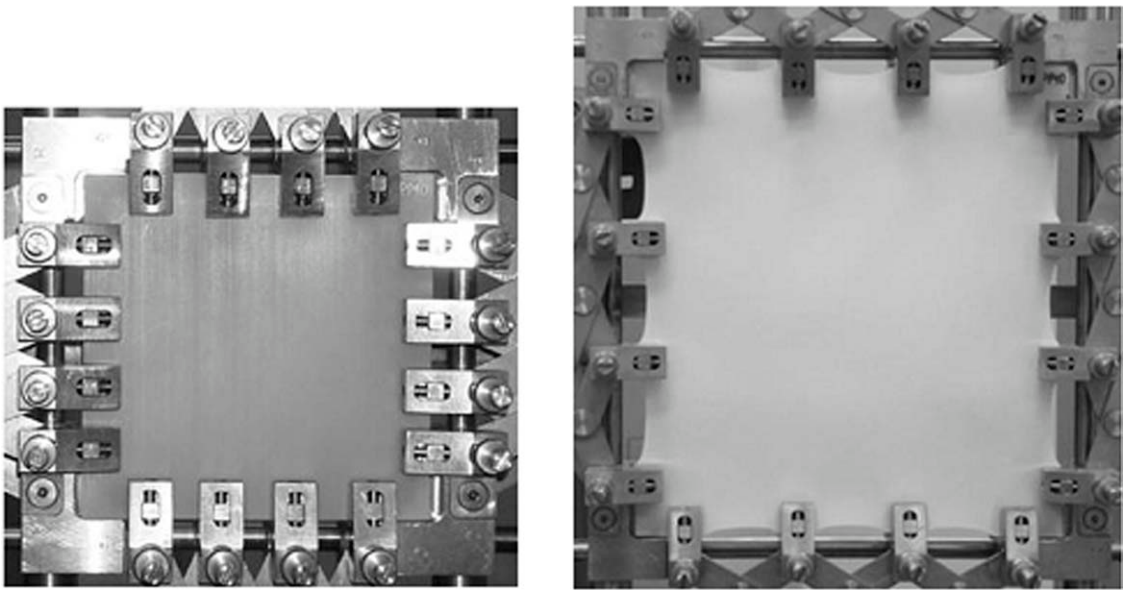

Figure 4 Film before and after stretching with the biaxial stretching module.[14]

TABLE II
Operating Conditions

	Temperature (°C)	Heating time (s) for films of 500-μm thickness	Longitudinal speed (VMD) (mm/s)	Surface gain (%)	Stretching ratio
PP	150	120	80	50–300	1
HDPE	110	90	80	50–300	1

Biaxial stretching

Samples of lateral dimensions 100 × 100 mm^2 and 500 μm in thickness suited for biaxial stretching were cut from the extruded and the calendared films. The biaxial stretching operation was carried out using a home-made module (Fig. 4), which is the subject of a patent request (Provisional request patent in USA No. 61/129, 127).[14] The stretching was applied simultaneously and the operating conditions in terms of temperature, heating time, longitudinal stretching speed (V_{MD}: velocity in the machine direction, MD), surface gain rate (%), and stretching ration (R) are reported in Table II. The temperature and time of heating were optimized using various experimental conditions.

The final porosity generated by the biaxial stretching depends on the experimental conditions such as temperature, heating duration, stretching speed, and draw ratio. Here, the temperature was selected owing to two criteria: (i) the required energy to reach decohesion at the matrix–particle interface should be lower than the energy necessary to deform the polymeric films plastically and (ii) the temperature should be lower than the melting point to avoid the collapse of the formed cellular structure. The extent of stretching is imposed by the draw ratio level that generates a given surface gain rate of stretching that characterizes the gain in surface by biaxial stretching, which is given by:

$$Te\% = \frac{S_f - S_i}{S_i} \times 100, \quad (3)$$

where S_i and S_f are the surface of the sample before and after stretching, respectively.

Porosity measurements

The porosity was evaluated via both the mercury porosimetry and scanning electron microscopy techniques. The crystallinity was determined to establish the contribution of the crystalline phase to the porosity created by biaxial stretching.

The mercury porosimetry was carried out using PoreSizer 9320 porosimeter equipment and the applied pressure varied between 0.45 and 29,000 psi. The operating conditions in terms of mercury intrusion pressure and depressurization are illustrated in Table III. Each incremental pressure was maintained during 10 s for stabilization.

The morphology of the samples was visualized by scanning electron microscopy using JSM-840A Electron Microscope under 15 kV. Before visualization, the surface of the samples was coated under vacuum with a gold-palladium to avoid surface charging.

The crystallinity measurement was carried out of using XRD Bruker in the wide angle mode reflection, and the X-ray spectra were analyzed using Topas program. The determined percentage of crystallinity is given by:

$$\% \text{ Crystallinity} = \frac{S_c}{S_c + S_a} \times 100, \quad (4)$$

where S_a and S_c are the areas of the amorphous and the crystalline zones, respectively.

RESULTS AND DISCUSSION

During biaxial stretching, the effort produced by the machine was recorded for each displacement in its direction (MD). Figure 5 reports the effect of $CaCO_3$ concentration on the variation of the load with the stretching ratio, the biaxial elastic modulus as function of the percentage of $CaCO_3$, and the variation of the involved loading work to reach 65-mm displacement in the MD, which corresponds to 200% surface gain rate for the two polymer matrices, HDPE and PP as a function of the percentage of $CaCO_3$.

TABLE III
Procedure for the Applied Pressure

Pressurization							
Total pressure (Psi)	0.45–30	30–450	450–1200	1200–2000	2000–5000	5000–10,000	10,000–29,000
Incremental pressure (Psi)	0.25	25	50	100	250	500	1000
Depressurization							
Total pressure (Psi)	29,000–10,000	10,000–8000	8000–1000	1000–400	400–100	100–24	
Incremental pressure (Psi)	−1000	−500	−250	−100	−50	−25	

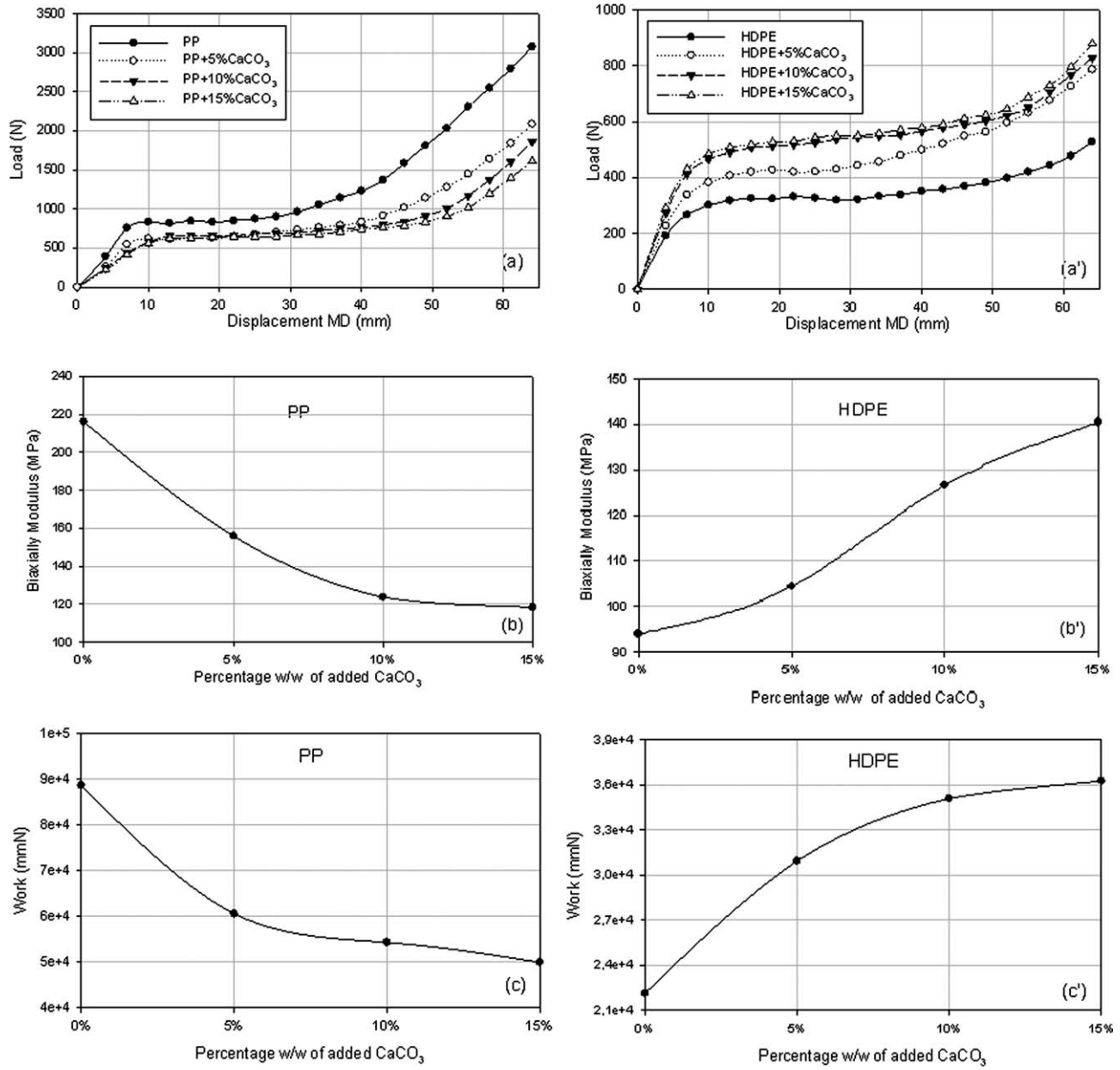

Figure 5 Plot of Load versus the displacement in machine direction (MD), biaxially modulus versus percentage w/w of added $CaCO_3$ and work versus percentage w/w of added $CaCO_3$, (a–c) PP matrix, and (a′–c′) HDPE matrix.

The results show that in the case of HDPE matrix, an increase in both modulus and total load is obtained upon increase in $CaCO_3$ concentration; a behavior similar to that exhibited by classical polymer composites, in which the particles act as reinforcement fillers. However, in the case of PP matrix, an opposite behavior is observed, with a decrease in mechanical properties upon the increase in the percentage of $CaCO_3$ particles. This unusual behavior suggests a preliminary interpretation related to the formation of pores due to interfacial decohesion between the matrix and particles. In fact, one of the crucial challenges in generating well-dispersed cellular structures by biaxial stretching is to find a polymer–particle system in which the particles disperse well within the polymeric matrix, while having at the same time poor interfacial adhesion with the matrix. Such contradictory requirements might be fulfilled by selecting the polymer matrix and the particles with solubility parameters that are different enough to have weak interfacial specific interactions and thus to generate interfacial decohesion during stretching, but close enough to ensure relatively good particles dispersion and distribution within the polymer matrix. For studied in the present work, the solubility parameters calculated by the Fedor method[15–19] are $\delta_{HDPE} = 7.9\ cal^{1/2}cm^{-3/2}$ for HDPE, $\delta_{PP} = 8.2\ cal^{1/2}cm^{-3/2}$ for PP, and $\delta_{CaCO_3} = 7.5\ cal^{1/2}cm^{-3/2}$ for $CaCO_3$. This means that better

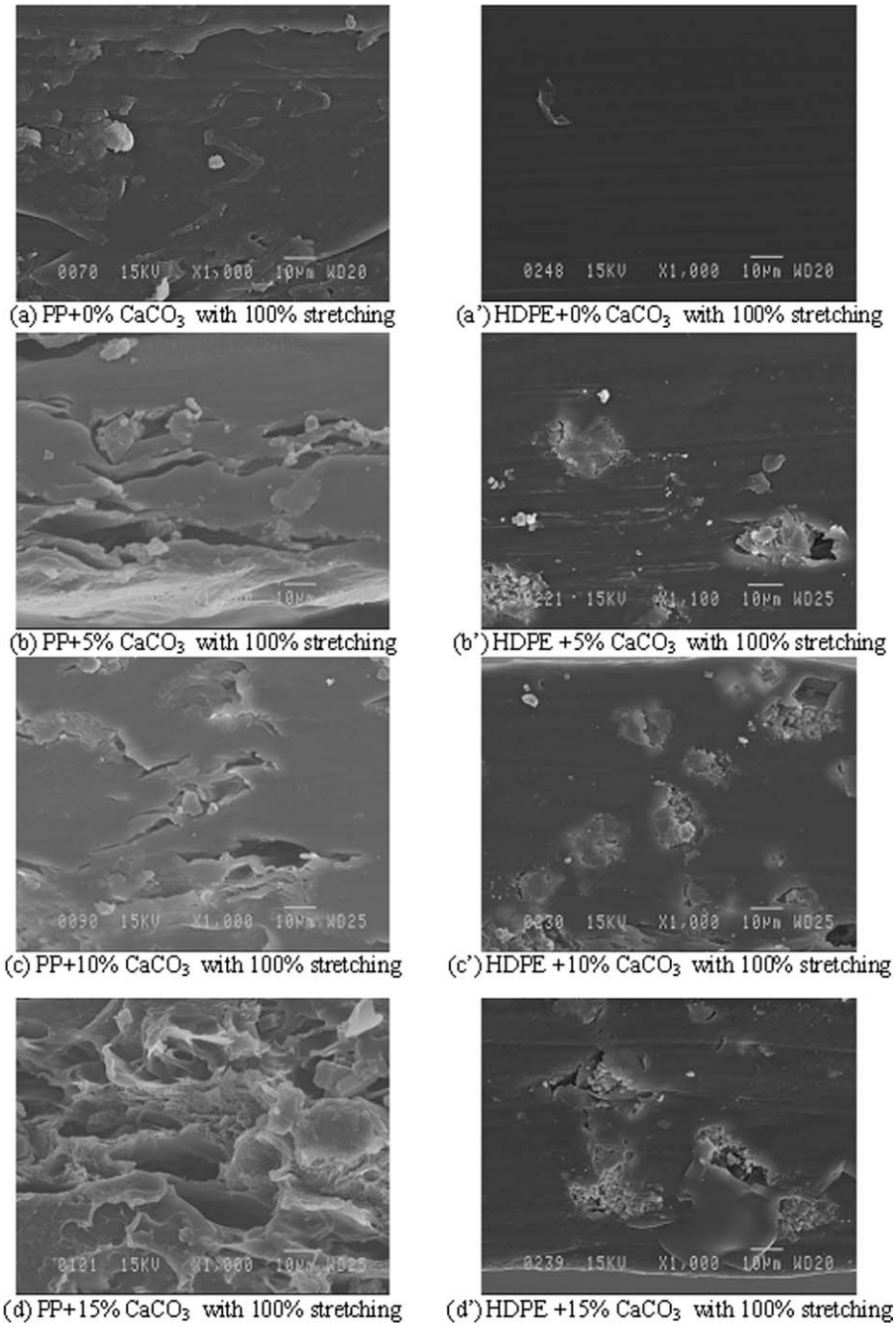

Figure 6 Scanning electron micrographs of a cross section of films with different percentages w/w of added $CaCO_3$ stretched at 100% surface gain rate. (a–d) PP matrix, (a′–d′) HDPE matrix. The films were fractured under liquid nitrogen.

dispersion and interfacial adhesion are expected more for HDPE than for PP. However, the difference in the solubility parameters of PP and $CaCO_3$ is not too big, and thus, one expects medium-type of dispersion along with weak interfacial adhesion that favors particle–matrix interfacial decohesion and thus the formation of cellular structure around agglomerate of particles. Of course the number and the dimensions of the cells are expected to increase with the biaxial draw ratio. This is confirmed by the scanning electron microscope observations shown in Figures 6 and 7. The figures also show that for the same particles loading and the same draw ratio, the cellular structure is more developed for PP than for HDPE-based composites. The micrographs show that a better interfacial adhesion is obtained for HDPE matrix, whereas in the case of PP matrix, cracks and voids develop rapidly at the surface of particles (or agglomerate of particles) even for small $CaCO_3$ loading. The number and the dimension of the voids increase with both $CaCO_3$ concentration and with the draw ratio.

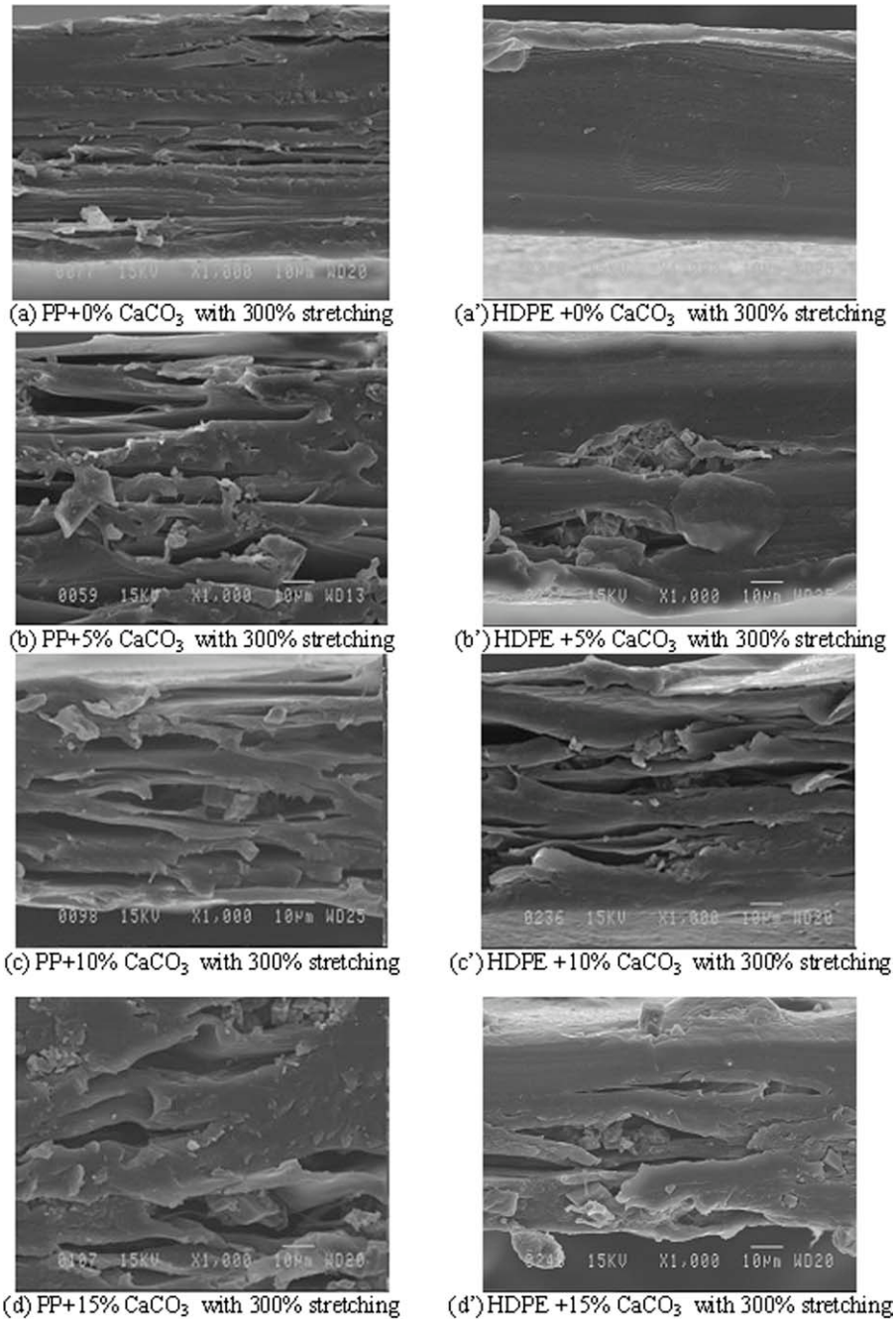

Figure 7 Scanning electron micrographs of a cross section of films with different percentages w/w of added $CaCO_3$ stretched at 300% surface gain rate. (a–d) PP matrix, (a′–d′) HDPE matrix. The films were fractured under liquid nitrogen.

The variation in the thickness reduction ratio as a function of the surface gain rate and the concentration of $CaCO_3$ particles is reported in Figure 8. For comparison purposes, the figure also reports the theoretical curve of thickness reduction assuming constant volume of the film during the biaxial stretching using

$$Tr\% = \frac{E_i - E_f}{E_i} \times 100, \quad (5)$$

where E_i and E_f are the thicknesses of the sample before and after stretching, respectively. The depth control was carried out using a dual gauge assembled on a magnetic base allowing the measurement of the film thickness in several positions. The reported thickness is the average value of the measurements taken at different positions.

The experimental results for PP-based composites show that the thickness reduction ratio decreases with increasing the percentage of $CaCO_3$ particles, whereas the inverse situation is observed for the HDPE case. The effect of particles concentration induces only a small increase in the thickness

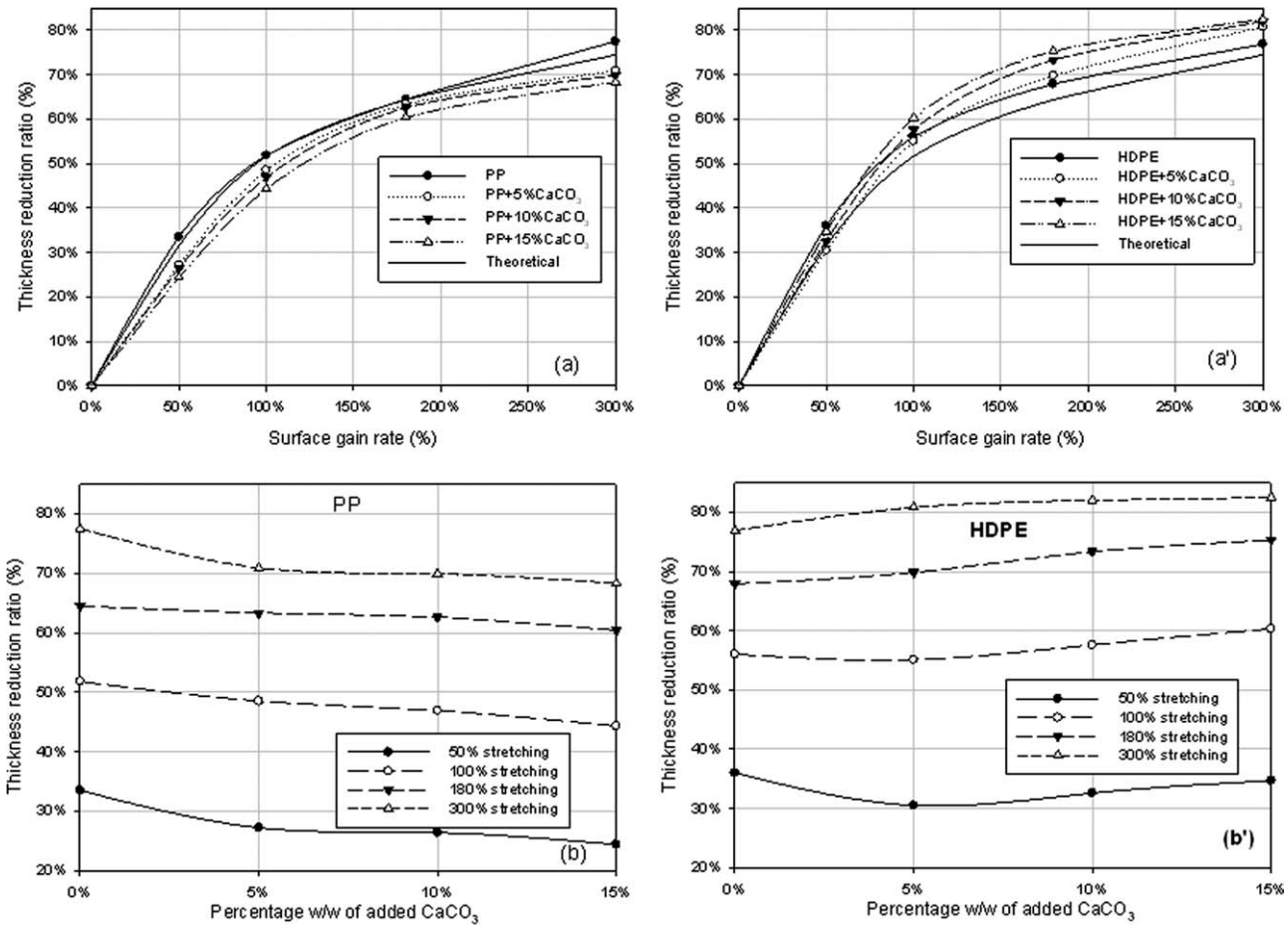

Figure 8 Plot of thickness reduction versus surface gain rate and percentage w/w of added $CaCO_3$ (a,b) PP matrix and (a′,b′) HDPE matrix.

reduction ratio for surface gain rate up to 100%. Above 120% of gain rate, the thickness reduction ratio shows an important increase with the concentration of the particles. These results have to be related to both swelling due to cellular structure and to the change in the samples crystallinity with both the $CaCO_3$ concentration and the percentage of the draw ratio. In fact, as aforementioned, PP-based composites show larger cellular structure, and thus, the films after biaxial stretching are characterized by a larger thickness than in the case of HDPE-based composites. The crystallinity of both PP- and HDPE-based composites are reported in Figure 9 for the same $CaCO_3$ concentration and for the same surface gain rate as those reported for thickness reduction. It is seen that the crystallinity of virgin PP first decreases and then increases with the increase in the draw ratio due the chains alignment during stretching. Upon addition of $CaCO_3$ particles, the variation of the crystallinity with the surface gain rate shows the same trend as for virgin PP, but with a decreased magnitude due the presence of voids that hinder the formation of aligned chains. In the case of HDPE-based composites, the crystallinity decreases with the draw ratio, and this is not contradictory with chains alignment. In fact, one has to contrast biaxial stretching with uniaxial stretching, and in the later case, one expects an increase in the crystallinity due the collective alignment of the chain units in the direction of stretching, whereas in biaxial stretching, the lateral deformation perturbs the uniaxial alignment that generates a decrease in local density and an increase in the amorphous phase. Such a mechanism is somewhat similar to the deformation-induced disentanglement, but here the biaxial deformation separates the chains that find difficulty for coming in close vicinity and align. The net result is a decrease in the total crystallinity of HDPE with the surface gain rate percentage. The same thing happens for virgin PP for small draw ratio but upon increase in the draw ratio, the local van der Waals specific interactions with the additional methyl groups that exist in PP and not in HDPE inhibit the later deformation and preserve the uniaxial alignment. With the addition of 5 and 10% of $CaCO_3$ particles the crystallinity of HDPE-based composites increases due to the effect of particles that play the role of nucleation sites for the crystallization. Such a

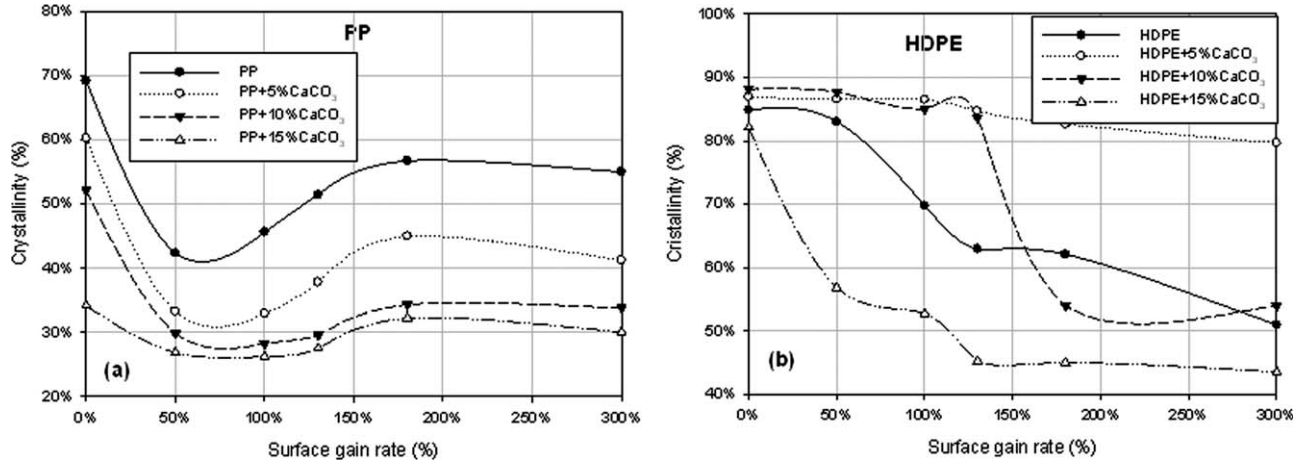

Figure 9 A plot of crystallinity versus surface gain rate in various percentage w/w of added $CaCO_3$, (a) PP matrix and (b) HDPE matrix.

situation occurs for surface gain rate up to 120%, after that the crystallinity decreases due to the formation of voids induced by stretching. For 15% of $CaCO_3$ particles in HDPE, the large aggregates overcome the effect of particle-induced crystallization.

The results of the porosity measurements are reported in Figures 10 and 11 in terms of the variation of the cumulated volume with the increase either in the surface gain rate or with the percentage of $CaCO_3$ particles.

Figures 10 and 11 reveal different features for the two polymer matrices, HDPE and PP. In the case of unstretched films, the percentage of added $CaCO_3$ particles did not have a significant influence neither on the cumulated volume nor on the porosity ($\sim$ 7%), which demonstrates that the large part of the porosity is mainly generated by the biaxial stretching. However, a small portion of voids of few nanometers in size did exist before stretching or loading with $CaCO_3$ particles. Such small voids are to be connected with the intrinsic free volume. Upon stretching, such a volume increases only very slightly in the case of PP due to eventual disentanglements and remains quite unchanged in the case of HDPE that shows lower free volume due to its high crystallinity (high local density). Upon loading with $CaCO_3$ particles and with stretching, interfacial decohesion generates additional macroscopic pores with a total porosity reaching $\sim$ 53% in PP-based composite films under conditions of 300% surface gain rate and 15% of added $CaCO_3$ particles, with a density of around 0,46 g/cm^3.

Figure 10 shows that the cumulative volume of PP-based composites increases as the pressure of the mercury is increased due to its infiltration in both macroscopic and microscopic pores and tends to reach the beginning of a pseudoplateau for large pressures corresponding to small pores of about 100 nm. The magnitude of such a pseudoplateau increases with the percentage of $CaCO_3$ loading. The final porosity in PP-based composite films increases with both surface gain rate and with the percentage of $CaCO_3$ loading.

In the case of HDPE-based composite films, there is a rapid increase in the cumulative volume with the pressure for reaching a plateau that spans over a wide range of pore sizes before slightly increasing again for small pore sizes. The value of the cumulative volume is however much smaller than in the case of PP-based composite films, in line with the expected smaller porosity for HDPE-based composite films. The maximum attained porosity is $\sim$ 18% recorded for a percentage of $CaCO_3$ particles of 10 and 300% of surface gain rate, with a generated density of 0.75 g/cm^3. This has to be related to the variation in the percentage of crystallinity with the $CaCO_3$ concentration shown in Figure 11. In fact PP-based composite films with 10% of $CaCO_3$ present a small difference in the percentage of crystallinity with respect to those with 15% of $CaCO_3$. However, in the case of the HDPE-based composite, films with 10% of $CaCO_3$ particles show larger crystallinity than films with 15%. The crystallinity contributes in fact to the porosity formation during the biaxial stretching, where the interface between the amorphous and the crystalline phases is a privileged location for the stress concentration. The porosity percentage of the HDPE-based composite films is very low, and the density is very high compared with the values recorded for films with PP matrix, which is in line with the reported results on mechanical properties, morphology, and crystallinity.

It is important to note that for PP-based films, the majority of the mercury volume intruded into the pores is observed for pore dimensions ranging from 0.01 to 1 μm (Fig. 10), despite the fact that the estimated pore dimensions for PP films lies between 50 and 100 μm. This discrepancy is due to the fact that

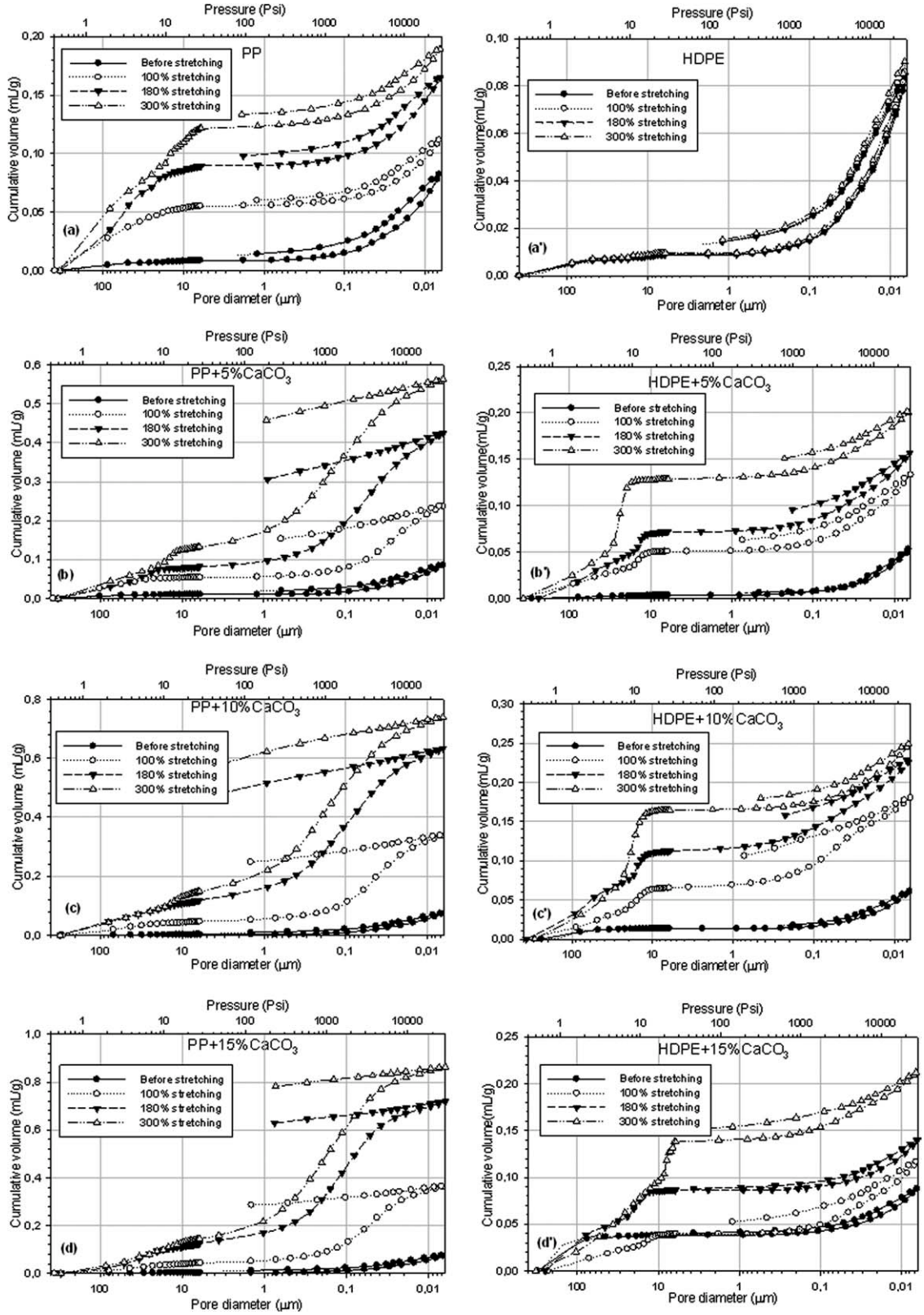

Figure 10 A plot of cumulative Volume versus pore diameter, (a–d) PP matrix with 0, 5, 10, and 15% $CaCO_3$. (a′–d′) HDPE matrix with 0, 5, 10, and 15% $CaCO_3$.

the calculations in mercury porosimetry are based on cylindrical pore geometry, and the detection is only possible if the pores are accessible and connected to the film surface. Here, the pressure was raised to high values reaching 29,000 psi, which allows mercury to reach the large non-

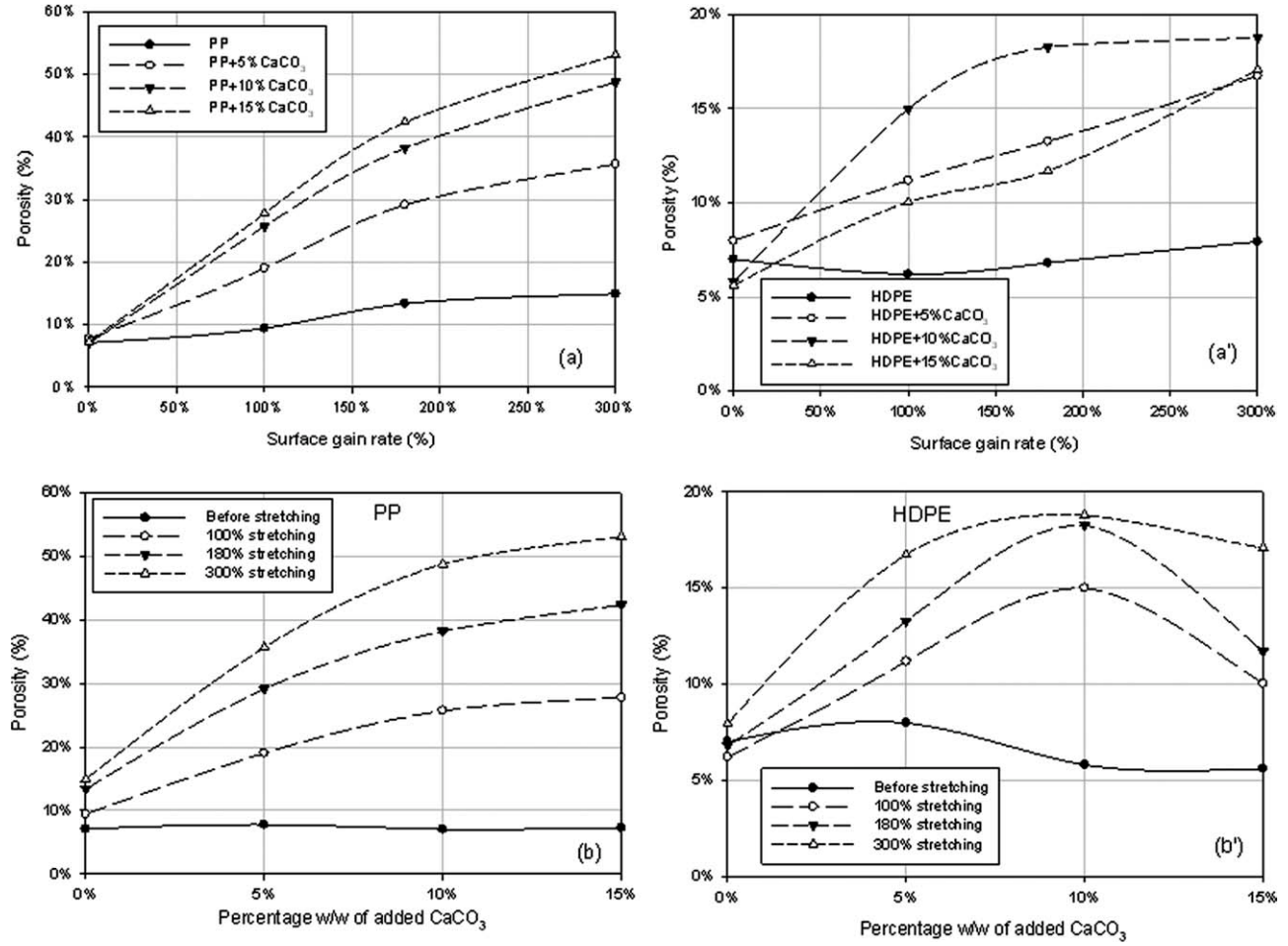

Figure 11 A plot of porosity percentage versus the surface gain rate and percentage w/w of added $CaCO_3$. (a,b) PP matrix and (a′,b′) HDPE matrix.

interconnected pores by forced permeation through intrinsic free volume (Fig. 12), and therefore, the measured pore diameter reflects in fact the diameter related to the diffusion pathways. The detection of these very small size pathways needs a high pressure for mercury intrusion. Furthermore, as the closed pores cannot be detected by the porosimetry measurements, the true value of porosity is certainly higher than the measured one. It should also be pointed out that the pore diameter distribution was not taken into account here.

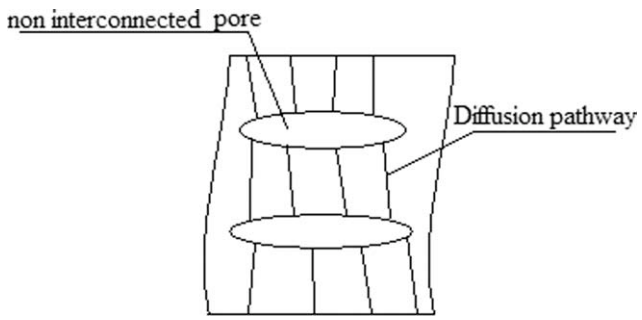

Figure 12 Diagram of mercury diffusion pathway.

The percentage of such interconnections can be estimated by noting that on decreasing the pressure, the curve of the cumulative volume versus pore

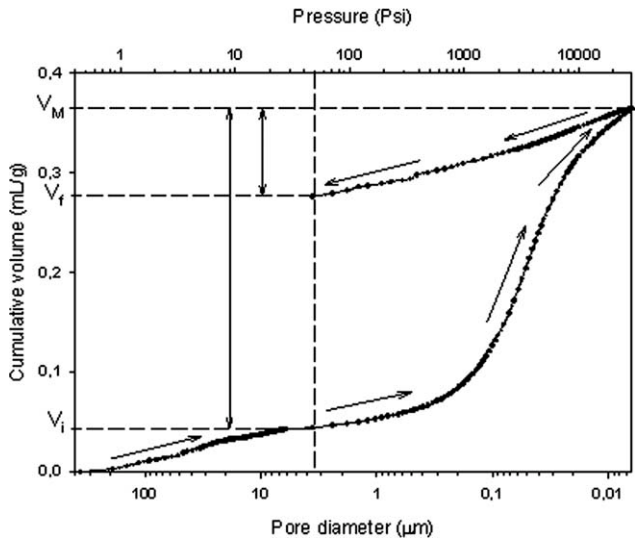

Figure 13 A plot of cumulative Volume versus pore diameter and intrusion pressure.

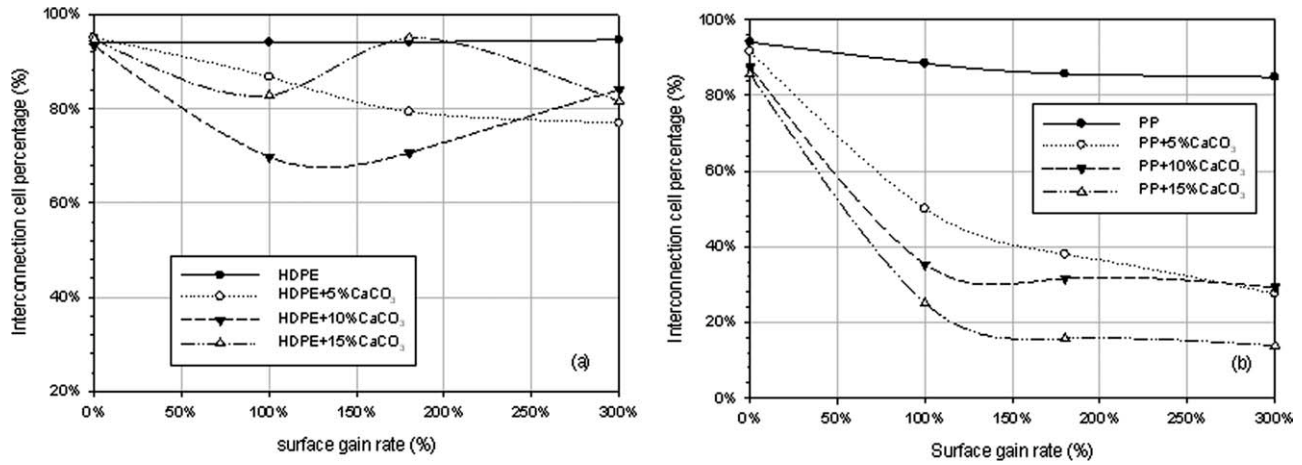

Figure 14 A plot of interconnection cell percentage versus surface gain rate and percentage w/w of added $CaCO_3$ for (a) HDPE matrix and (b) PP Matrix.

diameter shows a hysteresis as indicated in Figure 10. By decreasing the pressure, the mercury comes out from the pores, mainly at the surface. The remaining mercury volume allows the determination of the interconnections percentage as shown on Figure 13 using the following relationship:

$$It(\%) = \frac{V_M - V_f}{V_M - V_i} \times 100 \quad (6)$$

The results reported in Figure 14 show that the interconnection cell percentage for PP matrix is lower than the one for HDPE and the maximum percentage of non-interconnected porous structure is around 85% for PP-based composites with 15% of $CaCO_3$ particles and a surface gain rate between 150 and 300%.

CONCLUDING REMARKS

PP- and HDPE-based composites filled with various concentrations of $CaCO_3$ particles have been stretched biaxially at various stretch ratios using a home-developed stretching device connected to a classical mechanical testing machine. The stretching operation generated porous structure with an average porosity and density that were found to depend on the matrix nature, its crystallinity, and its specific interactions with the solid particles. It was found that PP matrix generates larger porosity compared to HDPE due to its low-interfacial adhesion with $CaCO_3$ particles. The variation in crystallinity during stretching plays also a major role. In the case of HDPE, the addition of $CaCO_3$ particles increases the crystallinity up to 10%, whereas in the case of PP matrix the crystallinity decreased. This is related to the biaxial nature of stretching that inhibits the one-directional orientation of the chains. This behavior was found to be more pronounced for HDPE than for PP for which specific van der Waals interactions between the methyl groups are likely to occur. Such a peculiar behavior impacted the cumulative porosity of the corresponding composites.

References

1. Zhang, X.; Hillenbrand, J.; Sessler, G. M. Appl Phys 2006, 84, 139.
2. Altafim, R. A. C.; Basso, H. C.; Altafim, R. A. P.; Lima, L.; Aquino, C. V. D.; Neto, L. G. IEEE T Dielect El In 2006, 13, 5.
3. Hillenbrand, J.; Behrendt, N.; Altstadt, V.; Schmidt, H. W.; Sessler, G. M. J Phys D: Appl Phys 2006, 39, 535.
4. Nagov, S.; Mizutani, Y. J Appl Polym Sci 1998, 68, 1543.
5. Hillenbrand, J.; Behrendt, N.; Mohmeyer, N.; Altstadt, V.; Schmidt, H. W.; Sessler, G. M. In Proceedings/12th International Symposium on Electrets, Piscataway, New Jersey, USA (ISE 12), 2005, p 276.
6. Behrendt, N.; Altstadt, V.; Schmidt, H. W.; Xiaoqing, Z.; Sessler, G. M. IEEE T Dielect El In 2006, 13, 5.
7. Montanari, G. C. IEEE T Dielect El In 2003, 10, 4.
8. Saarimaki, E.; Paajanen, M.; Savijarvi, A. M.; Minkkinen, H.; Wegener, M.; Voronina, O.; Schulze, R.; Wirges, W.; Multhaupt, R. G. IEEE T Dielect El In 2006, 13, 5.
9. Schwodiauer, R.; Graz, I.; Kaltenbrunner, M.; Keplinger, C.; Bartu, P.; Buchberger, G.; Ortwein, C.; Bauer, S. In Electroactive Polymer Actuators and Devices (EAPAD); Bar-Cohen, Y., Eds.; Proceedings of the 10th SPIE Electroactive Polymer Actuators and Devices (EAPAD) conference, March 2008, San Diego, California, USA, Proc. SPIE Vol. 6927.
10. Pilkey, W. D. Peterson's stress concentration, 2nd ed; Wiley-Interscience, 1997, Hoboken, New Jersey.
11. Neuber, H. Notch Stress Theory, Air Force Mat. Laboratory, Technical Report AFML 1965 TR-65–255.
12. Howe, D. V. Polymer Data Handbook; Oxford University, 1999, New York.
13. Mandelkern, L.; Alamo, R. G. Polymer Data Handbook; Oxford University, 1999, New York.
14. Qaiss, A.; Bousmina, M. U.S. Pat. Appl 61/129, 127 (2008).
15. Hilderbrand, J. H.; Scott, R. L. The Solubility of Non-Electrolytes, 3rd ed.; Reinhold: New York, 1959.
16. Dumont, M. J.; Reyna-Valencia, A.; Emond, J. P.; Bousmina M. J Appl Polym Sci 2007, 103, 618.
17. Ray, S. S.; Bousmina, M. Polymer 2005, 46, 12430.
18. El Mabrouk, K.; Bousmina, M.; Sinha Ray, S. J Nanosci Nanotechnol 2006, 6, 1.
19. Simha Ray, S.; Bousmina, M.; Maazouz, A. Polym Eng Sci 2006, 46, 1121.